LETTER

doi:10.1038/nature13454

A close-pair binary in a distant triple supermassive black hole system

R. P. Deane[1,2], Z. Paragi[3], M. J. Jarvis[4,5], M. Coriat[1,2], G. Bernardi[2,6,7], R. P. Fender[4], S. Frey[8], I. Heywood[6,9], H.-R. Klöckner[10], K. Grainge[11] & C. Rumsey[12]

Galaxies are believed to evolve through merging[1], which should lead to some hosting multiple supermassive black holes[2–4]. There are four known triple black hole systems[5–8], with the closest black hole pair being 2.4 kiloparsecs apart (the third component in this system is at 3 kiloparsecs)[7], which is far from the gravitational sphere of influence (about 100 parsecs for a black hole with mass one billion times that of the Sun). Previous searches for compact black hole systems concluded that they were rare[9], with the tightest binary system having a separation of 7 parsecs (ref. 10). Here we report observations of a triple black hole system at redshift $z = 0.39$, with the closest pair separated by about 140 parsecs and significantly more distant from Earth than any other known binary of comparable orbital separation. The effect of the tight pair is to introduce a rotationally symmetric helical modulation on the structure of the large-scale radio jets, which provides a useful way to search for other tight pairs without needing extremely high resolution observations. As we found this tight pair after searching only six galaxies, we conclude that tight pairs are more common than hitherto believed, which is an important observational constraint for low-frequency gravitational wave experiments[11,12].

SDSS J150243.09+111557.3 (J1502+1115 hereafter) was identified as a quasar at $z = 0.39$ with double-peaked [O III] emission lines, which can be a signature of dual active galactic nuclei (AGN)[13]. Adaptive optics assisted near-infrared (K-band) images reveal two components separated by 1.4 arcsec (7.4 kpc) and are referred to as J1502P and J1502S[14]. Integral-field spectroscopy determined that the double-peaked [O III] emission in the SDSS spectrum is explained by a 657 km s^{-1} velocity offset between J1502S and J1502P, which are dust-obscured and unobscured AGN, respectively. These two components were also observed as steep-spectrum radio sources ($\alpha < -0.8$, with flux density $S_\nu \propto \nu^\alpha$, where ν is the emission frequency) with the Jansky Very Large Array (JVLA) at 1.4, 5 and 8 GHz. The combination of the above results supported the discovery of a kiloparsec-scale dual AGN system[15].

We performed 1.7 GHz and 5 GHz Very Long Baseline Interferometry (VLBI) observations of J1502+1115 with the European VLBI Network (EVN), revealing two flat-spectrum ($\alpha \approx -0.1 \pm 0.1$) radio components within the spatially unresolved near-infrared component J1502S. Flat radio spectra identify optically thick radio emission, which is characteristic of the core of relativistic jets generated by an accreting black hole[16]. The two components (labelled J1502SE and J1502SW in Fig. 1a) are each marginally resolved and have an angular separation of ~26 mas, which corresponds to a projected spatial separation of ~138 pc at $z = 0.39$. Both J1502SE and J1502SW have radio luminosities of $L_{1.7} = 7 \times 10^{23}$ W Hz^{-1} and brightness temperatures of $T_B \gtrsim 2 \times 10^8$ K, consistent with actively accreting, intermediate radio luminosity nuclei. The high brightness temperatures, flat spectra, and co-spatial centroids (of both J1502SE and J1502SW) at both frequencies strongly support that these two radio components are associated with two separate, accreting supermassive black holes (SMBHs). Alternative scenarios are discussed and ruled out in the Methods section. Arcminute Microkelvin Imager (AMI) Large Array observations at 15.7 GHz suggest that the two radio cores (J1502SE/SW) flatten the overall J1502S spectrum at higher frequency (Extended Data Fig. 1). The third active nucleus (J1502P) at a projected distance of 7.4 kpc from J1502S has a steep radio spectrum and is not detected in the VLBI observations.

A re-analysis of archival JVLA observations provides supporting evidence for the inner binary discovery in J1502S. The JVLA 5 GHz map of J1502S and J1502P is shown in Fig. 1b, and Fig. 1c shows the point-source-subtracted JVLA 5 GHz residual map. The latter reveals 'S'-shaped radio emission detected at high significance and which is rotationally symmetric about the flat-spectrum nuclei (a larger version of Fig. 1c is shown in Extended Data Fig. 2). The 5 GHz inner-jet axis is offset by ~45° from the position angle of the vector between J1502SE and J1502SW (Extended Data Fig. 3). The location and close proximity of the two flat-spectrum nuclei support the view that the 'S'-shaped radio emission is a modulation (or bending) of one pair of jets associated with one of the nuclear components. This type of 'S'-shaped structure is commonly attributed to precessing jets, with a resulting radio-jet morphology similar to the famous X-ray binary SS 433[17]. Jet precession in AGN has long been predicted to be associated with the presence of binary black holes[3]. The spatially resolved detection of the inner binary centred on the 'S'-shaped jet emission provides, for the first time, direct evidence of this prediction. It therefore demonstrates that this is a promising method to find close-pair binary SMBHs that cannot be spatially resolved by current instruments ($\ll$1 mas angular resolution), yielding excellent targets for pointed gravitational wave experiments. The configuration where a primary black hole emits significant extended jet emission while the secondary appears to have none is also seen in the lowest-separation binary SMBH known, namely the VLBI-discovered system 0402+379 at $z \approx 0.06$ (ref. 10).

The host galaxies associated with J1502P and J1502S have elliptical galaxy morphologies and stellar masses of $M_* = (1.7 \pm 0.3) \times 10^{11}\ M_\odot$ and $(2.4 \pm 0.4) \times 10^{11}\ M_\odot$, respectively[15], where $M_\odot$ is the solar mass. J1502P has a measured black-hole mass (M_{BH}) given by $\log(M_{BH}/M_\odot) = 8.06 \pm 0.24$ (ref. 15), which is consistent with the black hole to bulge mass (M_{BH}–M_{bulge}) relation[18]. If the same is true for J1502S, this implies that J1502SE/SW both have M_{BH} values of $\sim 10^8\ M_\odot$ and each have a sphere of influence of ~10 pc (the radius at which the black hole dominates the gravitational potential relative to the host galaxy). The J1502S optical spectrum reveals a single [O III] component, despite the double flat-spectrum cores. If a circular orbit of radius $a = 138/2 = 69$ pc and a black hole binary mass M_{12} of $2 \times 10^8\ M_\odot$ are assumed, the maximum expected velocity offset between J1502SE/SW is $V_{J1502E/W} = \sqrt{GM_{12}/a}$

[1]Astrophysics, Cosmology and Gravity Centre, Department of Astronomy, University of Cape Town, Rondebosch, 7701, Cape Town, South Africa. [2]Square Kilometre Array South Africa, Pinelands, 7405, Cape Town, South Africa. [3]Joint Institute for VLBI in Europe, 7990 AA, Dwingeloo, The Netherlands. [4]Astrophysics, Department of Physics, University of Oxford, Oxford OX1 3RH, UK. [5]Physics Department, University of the Western Cape, Belville, 7535, South Africa. [6]Centre for Radio Astronomy Techniques and Technologies, Department of Physics and Electronics, Rhodes University, Grahamstown, 6140, South Africa. [7]Harvard-Smithsonian Center for Astrophysics, Cambridge, Massachusetts 02138, USA. [8]Satellite Geodetic Observatory, Institute of Geodesy, Cartography and Remote Sensing, H-1592, Budapest, Hungary. [9]Australia Telescope National Facility, CSIRO Astronomy and Space Science, Epping, New South Wales 1710, Australia. [10]Max-Planck-Institut für Radioastronomie, D-53121 Bonn, Germany. [11]Jodrell Bank Centre for Astrophysics, School of Physics and Astronomy, The University of Manchester, Manchester, UK. [12]Astrophysics Group, Cavendish Laboratory, University of Cambridge, Cambridge, UK.

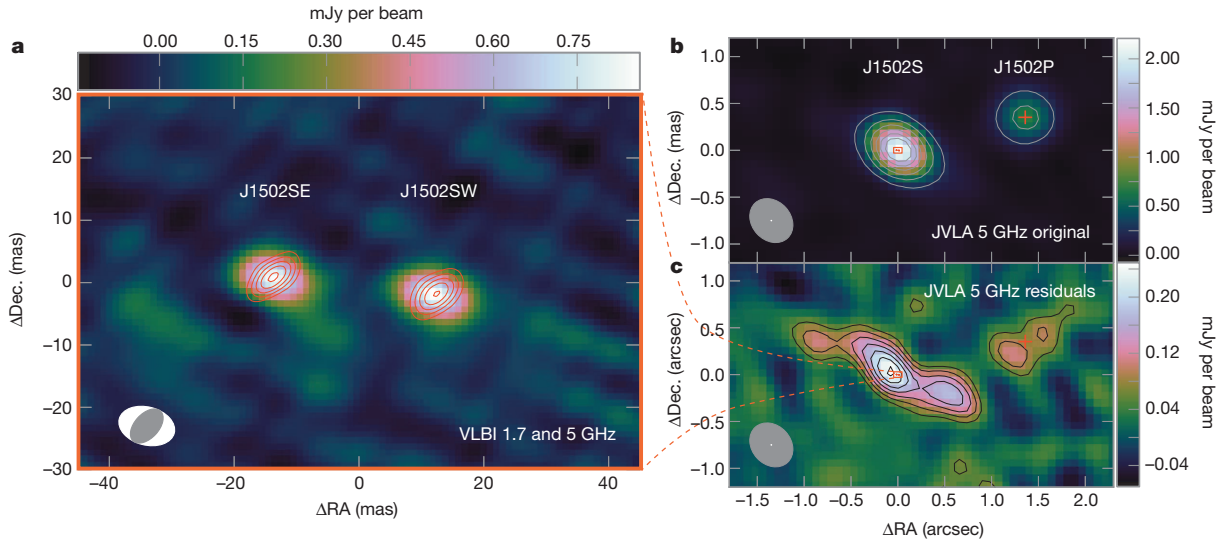

Figure 1 | VLBI and JVLA maps of the triple supermassive black hole system in J1502+1115. **a**, 5 GHz VLBI map (colour scale) showing the two components J1502SE and J1502SW. Over-plotted are red contours of the 1.7 GHz VLBI map with levels beginning at 400 μJy per beam and increasing in steps of 100 μJy per beam (~3σ). RA, right ascension; dec., declination. **b**, JVLA 5 GHz map imaged with Briggs uv-weighting (robust = 1; see discussion on weighting in Methods). Over-plotted are the 5 GHz contours (grey) starting at 250 μJy per beam and increasing in steps of 300 μJy per beam (20σ). **c**, Point-source subtracted JVLA 5 GHz residuals, revealing a rotationally symmetric 'S'-shaped radio emission centred on VLBI components (within the red rectangle). There also appear to be small-scale jets centred on the J1502P radio nucleus (red cross). Over-plotted are the JVLA 5 GHz contours (black) starting at 60 μJy per beam (4σ) and increasing in steps of 2σ. Also shown are the frame boundaries of the left panel. Negative contours are also shown at −4σ. The white ellipses in lower left of all three panels indicate the point spread function (PSF) full-width at half-maximum (FWHM) of the 5 GHz VLBI map. The grey ellipse in **a** shows the 1.7 GHz VLBI PSF, while the larger grey ellipses in **b** and **c** show the JVLA 5 GHz PSF.

≈110 km s^{-1}, which is within the measured J1502S [O III] line width of 384 km s^{-1}. Given that the original J1502+1115 selection was based on double-peaked [O III] lines separated by 657 km s^{-1}, it is clear that neither the double-peaked [O III] nor the double-cored near-infrared imaging played any part in the selection of the much closer binary SMBH within J1502S. This implies that the only major selection criteria for the close-pair binary within J1502S are K-band magnitude ($K \approx 14$–16 mag), redshift ($z \approx 0.1$–0.4) and integrated 1.4 GHz flux density ($S_{1.4} \approx 1$–60 mJy). Based on simulations for radio continuum sources[19], we expect a sky density of five such galaxies per square degree. Given that one sub-kpc binary was found from targeting six objects, this implies a sky density of $\Phi = 0.8^{+1.9}_{-0.7}$ per degree^2 for the given selection criteria, where we quote the formal Poisson 1σ uncertainties. Future VLBI surveys will be required to confirm this, given that the estimate is made from just six objects. While previous VLBI observations find a small fraction of binary/dual AGN[9], they typically target bright sources which are usually associated with the most massive black holes ($M_{BH} \gtrsim 10^9\ M_\odot$) for which there is a low probability of a similarly massive companion black hole.

To date, there are very few confirmed binary/dual AGN, despite the expectations from our understanding of hierarchical structure formation through galaxy merging, combined with the observational evidence that every massive galaxy hosts a central SMBH[20]. Of the binary/dual AGN with direct imaging confirmation, only three have sub-kpc projected separations and these systems are all at $z \lesssim 0.06$ (refs 10, 21, 22). In addition to these, there are a handful of candidate close-pair binaries based on light curve analyses, double-peaked broad lines and radio jet morphology[23–25], but these are not spatially resolved by current instruments. In Fig. 2 we show the projected spatial separations of the binary/dual AGN against redshift for a sample of sources that have been confirmed or discovered by spatially resolved X-ray, optical/infrared or radio imaging. While there may be a degree of subjectivity about which sources should appear in this list (some ambiguous cases have been omitted), it illustrates that the two VLBI-discovered systems have spatial

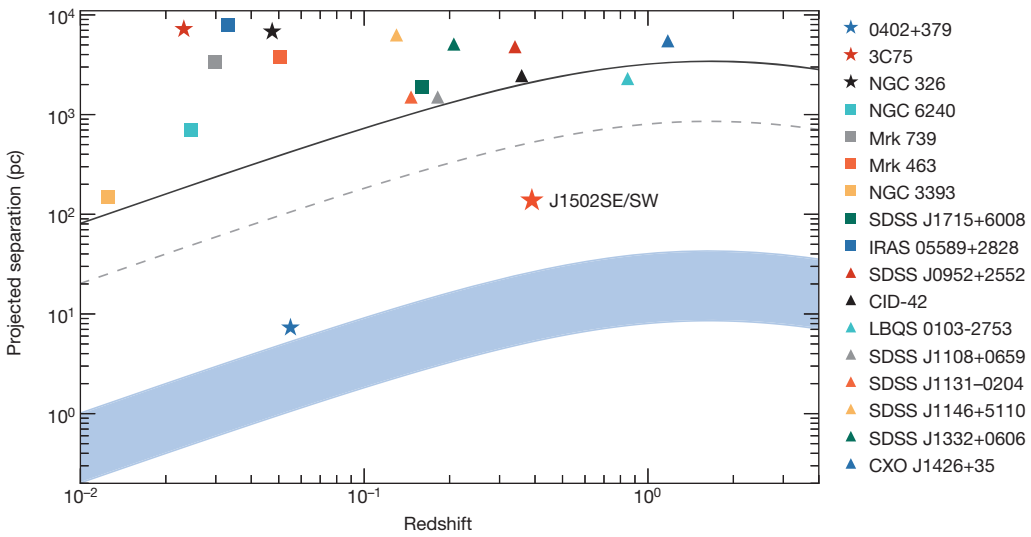

Figure 2 | Dual/binary AGN confirmed or discovered with direct imaging. Sample of binary/dual AGN confirmed or discovered by direct imaging at X-ray (squares), optical/infrared (triangles) and radio (stars) wavelengths. Typical spatial resolution limits of Chandra, the Hubble Space Telescope (HST) and VLBI are indicated by the solid and dashed lines, and shaded blue area, respectively. This illustrates that high-angular-resolution radio observations are able to survey a significantly larger cosmological volume for binary AGN with separations comparable to the black hole gravitational spheres of influence (<10 pc for $M_{BH} \approx 10^8 M_\odot$).

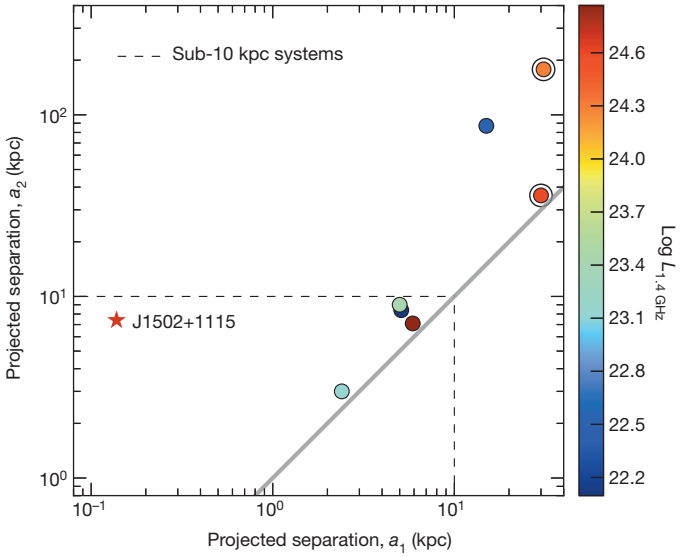

Figure 3 | Projected separations of candidate triple AGN. The axes denote the lowest (a_1) and second lowest (a_2) separations between AGN in the list of candidate triple AGN systems. The solid grey line indicates a ratio of unity. The dashed lines isolate the sub-10 kpc systems (see text). The colours correspond to the total integrated radio luminosity of the AGN plus the host galaxy (in units of W Hz^{-1}), since low-angular-resolution limits a fair AGN radio luminosity comparison. Nonetheless, the plot supports enhanced accretion within triple systems, particularly in the sub-10 kpc systems. J1502+1115 is an isolated region in the parameter space, probably owing to the bias against low separation for low-resolution optical/near-infrared and X-ray observations. The two black circled points (which are triple quasar systems) indicate upper radio luminosity limits from archival observations. The triple AGN candidates and their references are listed in Methods. Note that all sub-10 kpc systems are equidistant within a factor of 2, except for J1502+1115.

separations more than order of magnitude lower relative to X-ray and optical/infrared observations at similar redshifts. The J1502SE/SW binary has a period of $P_{bin} \approx 4$ Myr, assuming a circular orbit and major axis of 138 pc. This period is comparable to the lifetime of a typical radio source (~10 Myr).

Limited observational constraints exist on the abundance of triple black hole systems. There are only five triple AGN candidates with lowest (a_1) and second lowest (a_2) projected separations below 10 kpc ('sub-10 kpc systems' hereafter), which is the approximate effective radius for an elliptical galaxy. Figure 3 shows the lowest and second lowest projected separations for all the candidate triple AGN systems found in the literature (eight in total for separations $\lesssim$100 kpc). Six of the eight known triple systems (and all the sub-10 kpc systems) have associated radio emission with 1.4 GHz luminosities in the range $\log L_{1.4} \approx 22$–25 (here $L_{1.4}$ is in units of W Hz^{-1}). Like J1502+1115, some of these triple systems have radio emission associated with multiple nuclei. From the literature and archival data, we find that at least 9/15 (>60%) of the sub-10 kpc SMBHs have associated radio emission. This is a lower limit for two reasons: (1) sensitivity of the available observations; and (2) some of the radio imaging available does not have sufficient angular resolution to resolve all three galaxies or nuclear cores in a triple system. The fraction of triple AGN with associated radio emission is significantly higher than the typical value of ~10% for AGN[26], suggesting that triple systems lead to higher accretion activity and consequently a higher chance of jet triggering. None of the sub-10 kpc systems were selected on the basis of their radio emission, implying no clear biasing selection effects (see details of host galaxies in Methods). Evidence for enhanced accretion has also been found for ~10–100 kpc separation, hard-X-ray-selected dual AGN at low redshift[27]. This is consistent with hydrodynamical simulations that find peak accretion and AGN luminosity occurring at the smallest separations (<1–10 kpc)[28]. The above findings are therefore consistent with the expected disruption to gas dynamics caused by multiple black hole orbits.

Multiple SMBH in-spiral and recoil rates, as well as the resulting orbital eccentricities, are predicted to dominate the stochastic gravitational wave background spectrum in the nHz–μHz range[29,30]. Therefore, constraints on the number density of triple systems is important to refine the strategy of the future pulsar timing array experiments. This discovery demonstrates that high-angular-resolution radio observations have a unique advantage in searching for multiple black hole systems over large cosmological volumes, and therefore predicts that radio facilities like the Square Kilometre Array (as a stand-alone array or part of a VLBI network) will lead to a dramatic increase in the number of known low-separation (≪1 kpc) systems, as well as unresolved candidates for pointed gravitational wave experiments.

METHODS SUMMARY

J1502+1115 was observed at 1.7 and 5 GHz with the European VLBI Network. The 305 m Arecibo observatory was included in the 1.7 GHz observation. The 5 GHz observation used the e-VLBI technique, which performs real-time correlation. The correlation averaging time was 2 s and 4 s for the 5 GHz and 1.7 GHz visibilities respectively and we used 32 delay steps (lags) per sub-band. There were 4 × 8 MHz subbands observed in both left and right circular polarizations with two-bit sampling. Both observations used 4C39.25 as a fringe-finding source and the nearby (angular distance $\Delta\theta \approx 51$ arcmin) source J1504+1029 as a phase calibrator. Both maps have a brightness scale uncertainty of ~10%. The VLBI observations at 1.7 and 5 GHz were taken 18 months apart (and 23 months for the Arecibo run). The 5 GHz JVLA observations were performed in A-configuration and all details thereof are described in the literature[15]. We re-calibrated these data using the CASA software package and achieved flux densities consistent with previously published values[15], within the uncertainties. The residual map shown in Fig. 1c was generated by taking the median of 500 realizations of maps made by subtracting point sources directly from the JVLA 5 GHz visibilities. The point source positions and flux densities were derived from the VLBI 5 GHz components and the JVLA 5 GHz map for the J1502S and J1502P components, respectively. Each realization added a random offset in flux density and position, defined by their 1σ uncertainties and drawn from a Gaussian distribution, so that the effect of calibration and deconvolution errors on the residual structure could be constrained. The 5 GHz VLBI observation was made 11 weeks before the JVLA 5 GHz observation[15], limiting the uncertainty due to source variability in the comparison of the two.

Online Content Methods, along with any additional Extended Data display items and Source Data, are available in the online version of the paper; references unique to these sections appear only in the online paper.

Received 25 February; accepted 1 May 2014.
Published online 25 June 2014.

1. Springel, V. *et al.* Simulations of the formation, evolution and clustering of galaxies and quasars. *Nature* **435,** 629–636 (2005).
2. Volonteri, M., Haardt, F. & Madau, P. The assembly and merging history of supermassive black holes in hierarchical models of galaxy formation. *Astrophys. J.* **582,** 559–573 (2003).
3. Begelman, M. C., Blandford, R. D. & Rees, M. J. Massive black hole binaries in active galactic nuclei. *Nature* **287,** 307–309 (1980).
4. Kulkarni, G. & Loeb, A. Formation of galactic nuclei with multiple supermassive black holes at high redshifts. *Mon. Not. R. Astron. Soc.* **422,** 1306–1323 (2012).
5. Tonry, J. L. Constraints on the orbits of multiple nuclei in brightest cluster galaxies. *Astrophys. J.* **279,** 13–18 (1984).
6. Barth, A. J., Bentz, M. C., Greene, J. E. & Ho, L. C. An offset Seyfert 2 nucleus in the minor merger system NGC 3341. *Astrophys. J.* **683,** L119–L122 (2008).
7. Liu, X., Shen, Y. & Strauss, M. A. Cosmic train wreck by massive black holes: discovery of a kiloparsec-scale triple active galactic nucleus. *Astrophys. J.* **736,** L7 (2011).
8. Schawinski, K. *et al.* Evidence for three accreting black holes in a galaxy at z ~ 1.35: a snapshot of recently formed black hole seeds? *Astrophys. J.* **743,** L37 (2011).
9. Burke-Spolaor, S. A radio census of binary supermassive black holes. *Mon. Not. R. Astron. Soc.* **410,** 2113–2122 (2011).
10. Rodriguez, C. *et al.* A compact supermassive binary black hole system. *Astrophys. J.* **646,** 49–60 (2006).
11. Wyithe, J. S. B. & Loeb, A. Low-frequency gravitational waves from massive black hole binaries: predictions for LISA and pulsar timing arrays. *Astrophys. J.* **590,** 691–706 (2003).
12. Sesana, A. Systematic investigation of the expected gravitational wave signal from supermassive black hole binaries in the pulsar timing band. *Mon. Not. R. Astron. Soc.* **433,** L1–L5 (2013).
13. Smith, K. L. *et al.* A search for binary active galactic nuclei: double-peaked [O III] AGNs in the Sloan Digital Sky Survey. *Astrophys. J.* **716,** 866–877 (2010).

14. Fu, H., Myers, A. D., Djorgovski, S. G. & Yan, L. Mergers in double-peaked [O III] active galactic nuclei. *Astrophys. J.* **733,** 103–109 (2011).
15. Fu, H. *et al.* A kiloparsec-scale binary active galactic nucleus confirmed by the expanded Very Large Array. *Astrophys. J.* **740,** L44 (2011).
16. Blandford, R. D. & Königl, A. Relativistic jets as compact radio sources. *Astrophys. J.* **232,** 34–48 (1979).
17. Hjellming, R. M. & Johnston, K. J. An analysis of the proper motions of SS 433 radio jets. *Astrophys. J.* **246,** L141–L145 (1981).
18. Häring, N. & Rix, H.-W. On the black hole mass-bulge mass relation. *Astrophys. J.* **604,** L89–L92 (2004).
19. Wilman, R. J. *et al.* A semi-empirical simulation of the extragalactic radio continuum sky for next generation radio telescopes. *Mon. Not. R. Astron. Soc.* **388,** 1335–1348 (2008).
20. Kormendy, J. & Richstone, D. Inward bound—the search for supermassive black holes in galactic nuclei. *Annu. Rev. Astron. Astrophys.* **33,** 581–624 (1995).
21. Komossa, S. *et al.* Discovery of a binary active galactic nucleus in the ultraluminous infrared galaxy NGC 6240 using Chandra. *Astrophys. J.* **582,** L15–L19 (2003).
22. Fabbiano, G., Wang, J., Elvis, M. & Risaliti, G. A close nuclear black-hole pair in the spiral galaxy NGC3393. *Nature* **477,** 431–434 (2011).
23. Kaastra, J. S. & Roos, N. Massive binary black-holes and wiggling jets. *Astron. Astrophys.* **254,** 96–98 (1992).
24. Valtonen, M. J. *et al.* A massive binary black-hole system in OJ287 and a test of general relativity. *Nature* **452,** 851–853 (2008).
25. Boroson, T. A. & Lauer, T. R. A candidate sub-parsec supermassive binary black hole system. *Nature* **458,** 53–55 (2009).
26. Jiang, L. *et al.* The radio-loud fraction of quasars is a strong function of redshift and optical luminosity. *Astrophys. J.* **656,** 680–690 (2007).
27. Koss, M. *et al.* Understanding dual active galactic nucleus activation in the nearby Universe. *Astrophys. J.* **746,** L22 (2012).
28. Van Wassenhove, S. *et al.* Observability of dual active galactic nuclei in merging galaxies. *Astrophys. J.* **748,** L7 (2012).
29. Hoffman, L. & Loeb, A. Dynamics of triple black hole systems in hierarchically merging massive galaxies. *Mon. Not. R. Astron. Soc.* **377,** 957–976 (2007).
30. Blecha, L., Cox, T. J., Loeb, A. & Hernquist, L. Recoiling black holes in merging galaxies: relationship to active galactic nucleus lifetimes, starbursts and the M_{BH}-σ_* relation. *Mon. Not. R. Astron. Soc.* **412,** 2154–2182 (2011).

Acknowledgements We thank J. Magorrian, A. Karastergiou, S. Ransom and B. Fanaroff for discussions. The European VLBI Network is a joint facility of European, Chinese, South African and other radio astronomy institutes funded by their national research councils. e-VLBI research infrastructure in Europe was supported by the European Union's Seventh Framework Programme (FP7/2007-2013) under grant agreement number RI-261525 NEXPReS. The financial assistance of the South African SKA Project (SKA SA) towards this research is acknowledged. Opinions expressed and conclusions arrived at are those of the authors and are not necessarily to be attributed to the SKA SA. Z.P. and S.F. acknowledge funding from the Hungarian Scientific Research Fund (OTKA 104539). Z.P. is grateful for funding support from the International Space Science Institute.

Author Contributions R.P.D. was the Principal Investigator of the project and wrote the paper. Z.P. helped design, schedule, observe and calibrate the EVN observations as well as interpret the results. M.J.J. helped interpret the cosmological and astrophysical importance of the discovery and contributed significantly to the text. M.C. and R.P.F. helped in the binary SMBH interpretation and the physics thereof. S.F. calibrated the 1.7 GHz EVN observation and helped in the VLBI component interpretation. G.B. and I.H. helped with the technical aspects of the JVLA re-analysis and the subtle interferometric effects at play. H.R.K. helped in the VLBI and GMRT proposals and wrote the software to calibrate the GMRT observation. K.G. and C.R. observed and calibrated the 16 GHz AMI observations. All authors contributed to the analysis and text.

Author Information Reprints and permissions information is available at www.nature.com/reprints. The authors declare no competing financial interests. Readers are welcome to comment on the online version of the paper. Correspondence and requests for materials should be addressed to R.P.D. (roger.deane@ast.uct.ac.za).

METHODS

Observations using e-VLBI 5 GHz. J1502+1115 was observed at 5 GHz with the European VLBI Network using the e-VLBI technique on 12 April 2011 for approximately 1.5 h. The participating telescopes were Effelsberg (Germany), Jodrell Bank (Mk II, UK), Hartebeesthoek (South Africa), Sheshan (China), Medicina (Italy), Onsala (Sweden), Toruń (Poland), Yebes (Spain) and the phased-array Westerbork Synthesis Radio Telescope (WSRT, Netherlands). The data were streamed real-time to the EVN Data Processor at the Joint Institute for VLBI in Europe (JIVE) at a 1,024 Mbps data rate. The correlation averaging time was 2 s and we used 32 delay steps (lags) per sub-band. The coordinates used for correlation were the J1502+1115 1.4 GHz centroid determined from the Faint Images of the Radio Sky at Twenty-Centimeters (FIRST) survey[31]. J1502SE/SW are detected sufficiently near the phase centre ($\Delta\theta \lesssim 1.3$ arcsec) that time and bandwidth smearing losses are negligible. There were 4×8 MHz sub-bands observed in both LCP and RCP polarizations with 2-bit sampling. The initial clock searching was carried out before the experiment using the fringe-finder source 4C39.25. J1502+1115 was phase-referenced to the nearby ($\Delta\theta \approx 51$ arcmin) calibrator J1504+1029 for 1.3 min per 5 min calibrator-target cycle. The J2000 coordinates of the reference source (RA = 15 h 04 min 24.979782 s, dec. = +10° 29′ 39.19858″) were taken from the Very Long Baseline Array (VLBA) Calibrator Survey (http://www.vlba.nrao.edu/astro/calib/index.shtml) and have a positional uncertainty of ~0.02 mas. The resultant map has a Briggs-weighted (robust = 0) synthesized beam with a 9.1×6.1 mas^2 FWHM at a position angle of 76° east of north. The r.m.s. noise in the Briggs-weighted (robust = 0) 5 GHz map is ~36 μJy per beam and the brightness scale uncertainty is ~10%. The J1502P component is not detected in the VLBI observations with a 5σ upper limit of $S_{5\mathrm{GHz}} \lesssim 180$ μJy perbeam. Components J1502SE and J1502SW are detected with flux densities of $S_{5\mathrm{GHz}} = 857 \pm 49$ and 872 ± 49 μJy respectively, where the uncertainties are the quadrature sum of the fitting uncertainty and the r.m.s of the map measured ~2 arcsec from the phase centre. This e-VLBI observation was made 11 weeks before the JVLA 5 GHz observation[15], limiting the uncertainty due to source variability in the comparison of the two.

Observations using VLBI 1.7 GHz. Based on the detection of two compact components in the e-VLBI 5 GHz map, we observed J1502S at 1.7 GHz using the European VLBI Network. The observations were performed on 24 October 2012 and 13 March 2013. Antennas included in the VLBI array for the 2012 run were the same as the 5 GHz e-VLBI observations, as well as Urumqi (China) and the Russian KVAZAR Network stations Svetloe, Zelenchukskaya and Badary. The second epoch observations included the following antennas: Arecibo, Effelsberg, Jodrell Bank, Onsala, Medicina, Toruń, Noto and WSRT. J1502S was observed for approximately 3 h in total. The data were 2-bit sampled. The data in this case were recorded with Mark5As and correlated at a later time at JIVE. There were 128 delay steps per sub-band and the integration time was 4 s. The same fringe-finder, phase reference target and duty cycle was used as in the e-VLBI observation. The coordinates used for correlation were determined from the e-VLBI 5 GHz detection. The 1.7 and 5 GHz VLBI centroids are consistent within the fitting uncertainties ($\lesssim 1.5$ mas, 7.5 pc) for non-self-calibrated 1.7 GHz *uv*-data. Including the Arecibo baselines in the 1.7 GHz *uv*-data and self-calibrating all Arecibo baselines leads to a higher angular resolution and fidelity map, but with compromised absolute astrometry. The resultant offset is (ΔRA, Δdec.) = (0.55 mas, 3.15 mas). This shift is corrected for in the map shown of J1502SE/SW in the left panel of Fig. 1 of the main paper. The measured flux densities for self-calibrated and un-self-calibrated data are consistent within the fitting uncertainties. The naturally weighted map has an r.m.s of ~31 μJy per beam and a synthesized beam FWHM of 6.5×3.9 mas^2 at a position angle of −42° east of north. The J1502P component is not detected in the VLBI observations with a 5σ upper limit of $S_{1.7\mathrm{GHz}} \lesssim 170$ μJy perbeam. Components J1502SE and J1502SW are detected with flux densities of $S_{1.7\mathrm{GHz}} = 954 \pm 50$ and 920 ± 49 μJy respectively, where the uncertainties are the quadrature sum of the fitting uncertainty and the r.m.s of the map measured ~2 arcsec from the phase centre. The VLBI observations at 1.7 and 5 GHz were taken 18 months apart (and 23 months for the Arecibo run), yielding an apparent proper motion upper limit of $\Delta\mu \lesssim 5$ pc yr^{-1}.

Observations using Arcminute Microkelvin Imager (AMI) 16 GHz. J1502+1115 was observed on 6 December 2012 for 12 h by the AMI Large Array[32] for approximately 1.5 h. The telescope observes between 13.5 and 18 GHz in six spectral channels of 0.75 GHz bandwidth. The source J1504+1029 was observed for 100 s every 600 s for accurate phase calibration. Flux density calibration was performed using short observations of 3C 286 which were calibrated against VLA measurements[33]. The data were flagged and calibrated using REDUCE, a local software package developed for AMI. The calibrated data were then mapped and CLEANed in AIPS using the IMAGR task. The integrated flux density of the detection was $S_{\mathrm{int}} \approx 1.17$ mJy. The final thermal noise on the continuum map was 35 μJy per beam and a flux scale uncertainty of 5%. The map has not been corrected for the telescope primary beam response, which is well modelled by a Gaussian of FWHM 5.6 arcmin. The CLEAN restoring beam has a FWHM of 64×23 arcsec at a position angle of 9°. We do not expect confusion with other sources within this beam based on the higher resolution and sensitivity JVLA continuum 8 GHz map.

Observations using Giant Metrewave Radio Telescope (GMRT) 610 MHz. J1502+1115 was observed with the GMRT array on 17 December 2012 at 610 MHz for approximately 45 min. J1502+1115 was phase referenced to the nearby ($\Delta\theta \approx 51$ arcmin) calibrator J1504+1029. Amplitude calibration was performed using 3C 286. Data processing was performed with an automated calibration and imaging pipeline based on PYTHON, AIPS and PARSELTONGUE[34] which has been specially developed to process GMRT data. The full technical description of this calibration and imaging pipeline is extensive and is presented in detail elsewhere[35]. The integrated flux density of J1502+1115 at 610 MHz is $S_{\mathrm{int}} = 22.84 \pm 0.95$ mJy, where the uncertainty is the quadrature sum of the fitting uncertainty and the local noise near the J1502+1115 detection. The CLEAN restoring beam is 5.5×4.4 arcsec at a position angle of 59°, and therefore does not spatially resolve J1502P and J1502S.

Observations using JVLA. The JVLA observations were performed on 29 June 2011 at 1.4 and 5 GHz. The 8 GHz observations were performed on 14 June 2011. All three of these bands were observed while the JVLA was in A-configuration. The details of the observations are reported in the literature[15]. We re-calibrated all three observations using the CASA software package and achieved flux densities consistent with previously determined values[15], within the uncertainties.

Radio spectra of radio components. In Extended Data Fig. 1 we show the radio spectra of the various components. The component J1502P has a steep spectrum and is unlikely to contribute to the measured 15.7 GHz AMI flux density. It therefore appears that the AMI map is dominated by the flat-spectrum cores.

JVLA 5 GHz residual map. The residual map shown in the bottom right panel of Fig. 1 was generated by taking the median of 500 realizations of maps made by subtracting point sources directly from the JVLA 5 GHz visibilities. The point source positions and flux densities were derived from the VLBI 5 GHz components (observed 11 weeks before the JVLA 5 GHz observation) and the Briggs-weighted (robust = 0) 5 GHz map of the JVLA 5 GHz data itself for the J1502S and J1502P components respectively. Each realization added a random offset in flux density and position, defined by their 1σ uncertainties and drawn from a Gaussian distribution, so that the effect of calibration and deconvolution errors on the residual structure could be constrained. Note the JVLA 8 GHz residual map shows similar structure, but at a lower signal-to-noise ratio. This analysis was performed using the MeqTrees software package[36] (www.meqtrees.net). The JVLA-detected jet emission is not detected in the VLBI maps, due to insufficient brightness temperature sensitivity.

JVLA 5 GHz inner jet. The JVLA residual map discussed above (and shown in Fig. 1c) was generated using Briggs weighing (robust = 1). In Extended Data Fig. 3, we show the same JVLA 5 GHz residuals but with Briggs weighting (robust = 0). This results in higher angular resolution (synthesized beam FWHM = 0.39×0.32 arcsec^2, position angle = 45° east of north), but with poorer sensitivity ($1\sigma \approx 30$ μJy per beam), or more importantly, poorer brightness temperature sensitivity. This results in a map that traces the higher brightness temperature emission which we use to probe the central region of J1502S (see Extended Data Fig. 3). This figure shows the JVLA 5 GHz inner jet at a position angle of ~45° east of north. This is significantly misaligned with the position angle of the vector between J1502SE and J1502SW ($\theta_{\mathrm{J1502SE/SW}} \approx 87°$). J1502SE is within ~20 mas of the brightest pixel in the JVLA 5 GHz residual map, well within the absolute JVLA astrometry of 100 mas[37]. This supports the view that the 'S'-shaped jet emission seen in Fig. 1c stems from one of the two VLBI-detected cores. The large misalignment is inconsistent with any scenario where the two VLBI components are interpreted as young hotspots stemming from a single, undetected core. Furthermore, the straight north-east inner jet with projected length ~0.4 arcsec (~2.1 kpc) and a jet axis position angle of ~45° is also inconsistent with a scenario where one of the VLBI components is an AGN core and the other a hotspot along the jet trajectory. A detailed discussion is also included in the following section.

Alternative interpretations of the parsec-scale radio emission in J1502S. In the two sub-sections below we distinguish between jets and hotspots to simplify comparison with the literature.

First, double-jet or core-jet scenarios. A possible interpretation of the double flat-spectrum structure of J1502S is that we observe the synchrotron self-absorbed bases of a pair of oppositely directed jets from a single AGN. Similar structures have been seen in nearby type-II AGN, as well as in the Galactic X-ray binary system SS 433[38]. We may exclude this scenario for a number of reasons. (1) We do not see elongated core-jet structure in either of the two components, which is contrary to what is typical of self-absorbed AGN cores. (2) We would not expect these to be unresolved at VLBI scales given the fact that the two components are separated by 26 mas, and the separation between the two jet sides should be comparable to the size of the core itself[16]. (3) The 138 pc physical separation between the two components is an order of magnitude larger than the typical size of radio cores (~1–10 pc) seen in the brightest AGN[39,40].

Second, double-hotspot or core-hotspot scenarios. There are a number of arguments against the scenario where the two compact J1502SE/SW components are hotspots as observed in the class of compact symmetric objects (CSOs); or alternatively that one component is a hotspot and the other the core. We outline the most important points. (1) Both components have flat spectra, which is uncharacteristic of hotspots which have typical spectral indices of $\alpha_{\rm hotspots} < -0.5$[41]. Spectral indices are even steeper for CSOs with a projected linear size (hotspot separation) greater than $\sim$100 pc[41]. (2) The population of CSOs have typical luminosities of 10^{27} W Hz^{-1}, which is 4 orders of magnitude larger than J1502SE/SW[41,42]. While this may be a selection effect, the lowest luminosity CSO that we have found in the literature has a 1.4 GHz radio luminosity that is 1 order of magnitude larger than that of J1502SE/SW[41]. (3) Similar to the double-jet/core-jet scenario discussed in the previous section, higher frequency observations probe nearer the base of the jet since it becomes optically thin closer to the central black hole[39,40]. In the core-hotspot scenario where the distance is as large as 138 pc, this would result in a observable frequency dependent core-shift (that is, decreasing separation between the two components) which we do not see: the separation of J1502SE and J1502SW appears independent of observing frequency. (4) In the double-hotspot scenario, there is no core emission detected (to $L_{1.7\rm GHz} \approx 10^{22}$ W Hz^{-1}). (5) The straight $\sim$2-kpc-long inner jet of J1502S has a 45° misalignment with the vector between J1502SE/SW. This would imply a dramatic, almost instantaneous change in angular momentum. (6) Assuming that one or both J1502SE/SW are young hotspots; this would imply that we happened to observe J1502+1115 within a very short time period since this dramatic change in angular momentum. If we assume that the jet axis is in the plane of the sky and a very conservative jet speed of 0.01–0.1c, the shift in momentum must have occurred within the last (2–20) $\times$ 10^3 yr. For a nominal radio source lifetime of $\sim 10^7$ yr, this represents a 0.02–0.2% probability. Indeed, hotspot velocities from young radio sources are typically 0.3–0.5c, and almost never below 0.1c, corroborating our claim that this is a very conservative estimate[41].

So in summary, in order for a core-hotspot or double-hotspot alternative to be true, the hotspot(s) would not only need to have highly uncharacteristic flat spectral indices (and potentially an order of magnitude larger core size compared to what is observed in the highest luminosity radio sources), but also to have been observed almost instantaneously after a major shift in angular momentum has occurred. Although the binary SMBH interpretation may be considered a (hitherto) exotic one, combining the above arguments with rotationally-symmetric 'S'-shaped flux strongly favours the binary SMBH interpretation.

Triple AGN candidates. The triple AGN candidates plotted in Fig. 3 of the main text and the relevant references are SDSS J1027+1749[7], NGC 3341[6,43], QQ 1429–008[44], GOODS J123652.77+621354.7[8], QQQ J1519+0627[45], NGC 6166[5,46] and the NGC 835 group[27]. The 1σ upper limits on 1.4 GHz radio luminosity for the two triple quasars are determined from the local noise estimate around their respective sky coordinates in VLA FIRST survey[31]. There is a broad range in redshifts for this list of triple AGN candidates spanning from $z \approx 0.005$ to $\sim$2. Primary host galaxy morphology does not appear to play a strong role in preferentially selecting the six triple AGN systems with radio emission (3 disks, 2 ellipticals, 1 cD).

31. Becker, R. H., White, R. L. & Helfand, D. J. The FIRST Survey: faint images of the radio sky at twenty centimeters. *Astrophys. J.* **450,** 559–577 (1995).
32. Zwart, J. T. L. *et al.* The Arcminute Microkelvin Imager. *Mon. Not. R. Astron. Soc.* **391,** 1545–1558 (2008).
33. Perley, R. A. & Butler, B. J. An accurate flux density scale from 1 to 50 GHz. *Astrophys. J.* **204** (Supp.), 19 (2013).
34. Kettenis, M., van Langevelde, H. J., Reynolds, C. & Cotton, B. in *Astronomical Data Analysis Software and Systems XV* (eds Gabriel, C., Arviset, C., Ponz, D. & Enrique, S.) 497–500 (ASP Conf. Ser. 351, Astronomical Society of the Pacific, 2006).
35. Mauch, T. *et al.* A 325-MHz GMRT survey of the Herschel-ATLAS/GAMA fields. *Mon. Not. R. Astron. Soc.* **435,** 650–662 (2013).
36. Noordam, J. E. & Smirnov, O. M. The MeqTrees software system and its use for third-generation calibration of radio interferometers. *Astron. Astrophys.* **524,** A61 (2010).
37. Ulvestad, J. S., Perley, R. A. & Chandler, C. J. VLA Observational Status Summary. https://science.nrao.edu/facilities/vla/docs/manuals/oss2013b/performance/positional-accuracy (2009).
38. Paragi, Z. *et al.* The inner radio jet region and the complex environment of SS433. *Astron. Astrophys.* **348,** 910–916 (1999).
39. Lobanov, A. P. Ultracompact jets in active galactic nuclei. *Astron. Astrophys.* **330,** 79–89 (1998).
40. Hada, K. *et al.* An origin of the radio jet in M87 at the location of the central black hole. *Nature* **477,** 185–187 (2011).
41. An, T. & Baan, W. A. The dynamic evolution of young extragalactic radio sources. *Astrophys. J.* **760,** 77 (2012).
42. O'Dea, C. P. The compact steep-spectrum and gigahertz peaked-spectrum radio sources. *Publ. Astron. Soc. Pacif.* **110,** 493–532 (1998).
43. Bianchi, S. *et al.* The NGC 3341 minor merger: a panchromatic view of the active galactic nucleus in a dwarf companion. *Mon. Not. R. Astron. Soc.* **435,** 2335–2344 (2013).
44. Djorgovski, S. G. *et al.* Discovery of a probable physical triple quasar. *Astrophys. J.* **662,** L1–L5 (2007).
45. Farina, E. P., Montuori, C., Decarli, R. & Fumagalli, M. Caught in the act: discovery of a physical quasar triplet. *Mon. Not. R. Astron. Soc.* **431,** 1019–1025 (2013).
46. Ge, J. & Owen, F. N. Faraday rotation in cooling flow clusters of galaxies. 2: Survey. *Astron. J.* **108,** 1523–1533 (1994).

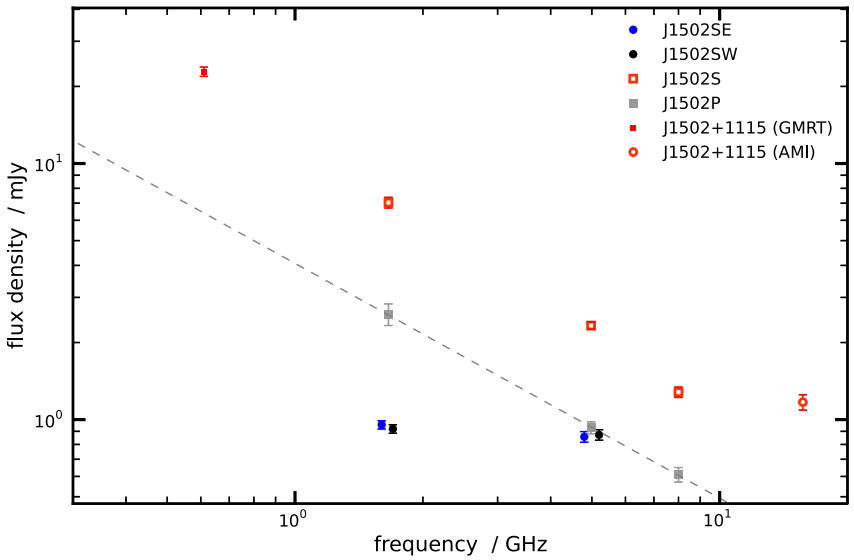

Extended Data Figure 1 | Radio spectrum of the radio components in J1502+1115. Both J1502S (open red squares) and J1502P (grey squares) are steep-spectrum radio sources between 1.4 and 8 GHz, as measured by JVLA observations. The two flat spectrum cores (J1502SE/SW, filled circles) are the likely cause of the flattened spectrum of J1502S at higher frequency, as measured by the AMI 15.7 GHz detection labelled as J1502+1115 (AMI). Error bars, ± 1s.d. on the flux measurement. J1502+1115 (GMRT) indicates the 610 MHz detection using the GMRT (Methods). Note that J1502SE and J1502SW are shown marginally offset in frequency purely for clearer illustration.

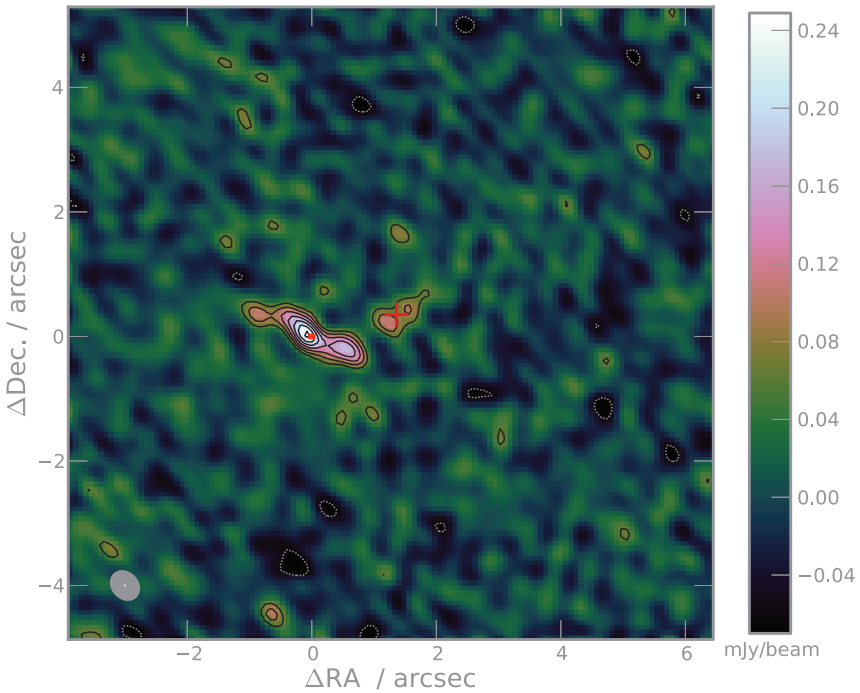

Extended Data Figure 2 | Larger field-of-view JVLA 5 GHz map of J1502+1115 to demonstrate map fidelity. The colour scale shows the same JVLA 5 GHz residuals shown in Fig. 1c but with the full 128 × 128 pixel median map generated from the Monte Carlo realizations. The small filled red square indicates the map boundary of the VLBI map shown in Fig. 1a. The red cross denotes the centroid of the point source subtracted J1502P component. Contour levels are the same as in Fig. 1c. The grey ellipse (lower left) represents the FWHM of the Briggs-weighted (robust = 1) PSF, while the white dot shows the VLBI 5 GHz PSF.

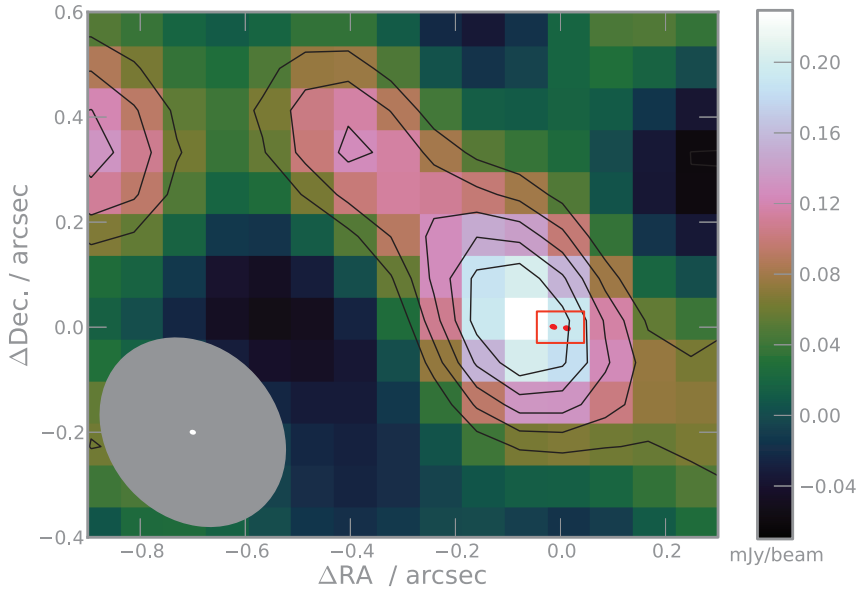

Extended Data Figure 3 | Zoom-in of the high-brightness-temperature inner jet emission of J1502S. The colour scale shows the same JVLA 5 GHz residuals shown in Fig. 1c but imaged with Briggs *uv*-weighting (robust = 0) to highlight the position angle of the inner northeast J1502S jet. This is misaligned with the vector between J1502SE and J1502SW (red dots) by ∼45°. The black JVLA 5 GHz contours start at 60 μJy per beam (∼2σ) and increase in steps of 1σ. The grey ellipse (lower left) represents the FWHM of the Briggs-weighted (robust = 0) PSF, while the white ellipse shows the VLBI 5 GHz PSF. The red square indicates the map boundary of the VLBI map shown in Fig. 1a.